Available online at www.sciencedirect.com
ScienceDirect
Nuclear Physics B Proceedings Supplement 00 (2014) 1–7
Nuclear Physics B Proceedings Supplement

J. Haser[a], on behalf of the Double Chooz collaboration

[a]*Max-Planck-Institut für Kernphysik, Heidelberg, Germany*

Abstract

The Double Chooz reactor antineutrino experiment aims for a precision measurement of the neutrino mixing angle θ_{13}. Located at the Chooz nuclear power plant in France, it observes an energy dependent deficit in the electron antineutrino spectrum, currently with one detector filled with gadolinium-loaded liquid scintillator at a baseline of 1.05 km. The Double Chooz analysis utilizes different approaches to extract θ_{13}: A combined rate and spectral shape fit as well as a background-model-independent analysis based on reactor power variations are performed, giving consistent results. Among the recent reactor-based oscillation experiments with comparable baseline it was the only one to observe reactor shutdown phases, during which all reactors are turned off. These enabled to measure the backgrounds solely, allowing to crosscheck the background models used in the oscillation analysis. At present an improved analysis was put forward with twice as much data statistics collected compared to the last publication. Revised selection criteria and background studies enhance the signal to background ratio while a decrease in the corresponding uncertainties is achieved. Along with an improved energy calibration the overall systematic uncertainty on θ_{13} is reduced, preparing for a two detector analysis. The new analysis obtains from 467.90 live days with 66.5 GW-ton-years of exposure (reactor power × detector mass × live time) a value of $\sin^2 2\theta_{13} = 0.090^{+0.032}_{-0.029}$ (stat + syst).

Keywords: Neutrino oscillation, mixing angle, reactor neutrino

1. Introduction

Based on the three-flavor framework, the neutrino oscillation probability can be described by three mixing angles, three mass squared differences and a CP-violating phase. The two mixing angles θ_{12} and θ_{23} were already known from several experiments [4], while θ_{13} remained unknown until reactor antineutrino and accelerator experiments succeeded to measure it in the recent years [2, 5, 6, 7, 8].

Since the mass-squared difference Δm_{21} is much smaller than Δm_{31}, electron antineutrino disappearance can be considered as a two-flavor oscillation. Together with the absence of matter effects, the survival probability is given by

$$P_{\bar{\nu}_e \to \bar{\nu}_e} \approx 1 - \sin^2 2\theta_{13} \cdot \sin^2 \left(1.27 \, \frac{\Delta m^2_{13}[\mathrm{eV}^2] \, L\,[\mathrm{m}]}{E_\nu\,[\mathrm{MeV}]} \right), \quad (1)$$

in case of a reactor antineutrino experiment at distances of a few hundred meter to about one kilometer from the reactor cores. The mixing angle θ_{13} can directly be obtained from a measurement of the neutrino deficit at ~ 1 km, with the current best result of $\Delta m^2_{31} = 2.44^{+0.09}_{-0.10} \times 10^{-3}$ eV^2 [9] as only additional input.

Electron antineutrinos with energies larger than 1.8 MeV can be detected via inverse beta decay (IBD) reaction on protons: $\bar{\nu}_e + p \to e^+ + n$. A prompt signal is created by the positron, carrying the information of the neutrino energy via $E_{\mathrm{signal}} \approx E_\nu - 0.8$ MeV. In the Double Chooz experiment is the neutron detected by means of radiative neutron capture within $\sim 30\,\mu$s, which is a competitive process mainly occurring on the rare earth element gadolinium (Gd) and hydrogen (H) nuclei present in the target liquid. Gd possesses very high cross-sections for the radiative capture of thermal neutrons, having a capture fraction of $\sim 85\,\%$ in the Double Chooz target scintillator.

Email address: julia.haser@mpi-hd.mpg.de (J. Haser)

Double Chooz has been the first reactor neutrino experiment providing a θ_{13} analysis using the neutron captures on H [3]. A combined analysis of both detection channels on H and Gd can be found in Ref. [10]. In this article the recent analysis based on the IBD detection channel with neutron captures on Gd is presented [1].

2. The Double Chooz Experiment

The Double Chooz (DC) experiment is located at the Chooz nuclear power station operated by EDF (Électricité de France) in the northeast of France. Each of the two pressurized water reactor cores provides 4.25 GW_{th} thermal power.

In the near future, DC will consist of two identical detectors: a near detector (ND) built to observe the neutrino source at 400 m distance with 120 m.w.e rock overburden and a far detector (FD) located 1050 km away from the reactor cores featuring 300 m.w.e overburden. Whereas the impact of θ_{13} is not yet observed in a neutrino flux measurement at the ND, the FD is placed near the first minimum of Eq. (1). The deficit in flux is hence obtained in a relative measurement and due to the identicalness of the detectors any correlated uncertainty between ND and FD will cancel out, allowing a precise determination of θ_{13}.

The DC experiment developed liquid scintillator detectors (Fig. 1), optimized to provide a calorimetric measure of the deposited energy upon neutrino interaction and to suppress backgrounds at the same time. Both detectors comprise four nested concentric cylinders, each filled with different liquids according to their function in the detection process. The *inner detector (ID)* is formed by the three innermost sub-volumes and represents the neutrino detector, which is optically separated from the other detector segments.

While any proton in form of a hydrogen nucleus acts as target for the IBD reaction, the fiducial volume of the oscillation analysis depends on the detection channel of the neutron produced by the neutrino interaction. Upon neutron capture on Gd, gammas with a total energy of ~ 8 MeV are produced, notably larger than the energies released in radioactive decays observed in nature, which enables to reduce the detection of accidental false coincidences. Hence for a Gd-based analysis the physical volume of neutrino detection is given by the *ν-target*, an acrylic vessel filled with 10.3 m^3 gadolinium-loaded liquid scintillator (1 g/L of Gd), located at the very center of the ID. It is surrounded by the *gamma-catcher* volume, a 55 cm thick layer (22.5 m^3) of gadolinium-free

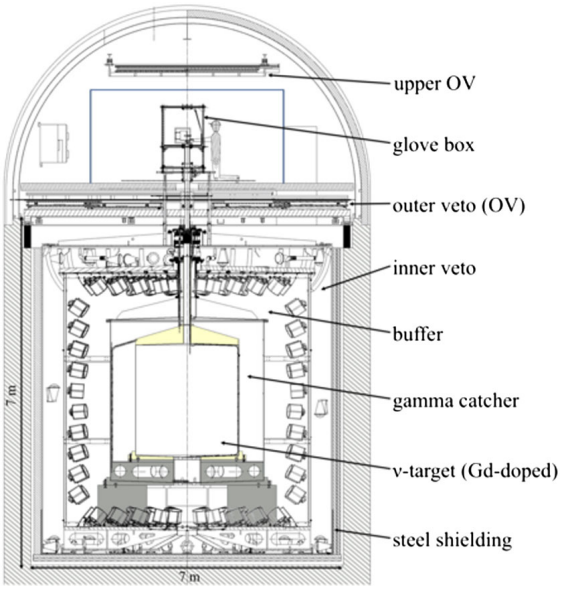

Figure 1: The Double Chooz detector design.

scintillator enclosed in an acrylic tank. Gammas produced by the IBD interactions are detected by both the *ν-target* and *gamma-catcher* volume, creating scintillation light. The next layer is formed by the *buffer*, which is equipped with 390 photomultiplier tubes (PMTs) of 10 inch size mounted on the stainless steel walls to collect the scintillation photons. The buffer is filled with non-scintillating mineral oil, building a 105 cm thick layer serving as a shield to radioactivity originating from the PMTs or the surrounding rock. The ID is surrounded by the fourth volume containing 90 m^3 of liquid scintillator and 78 eight inch PMTs, the *inner veto (IV)*. It is one of the two active muon vetoes of the DC experiment, used to identify and reject muons or muon-induced backgrounds. In the far detector are ID and IV protected from external gamma rays by a 15 cm thick steel shield built around the IV volume. On top of the cylindrical detector the second muon veto is installed. Consisting of perpendicular aligned plastic scintillator strips, the *outer veto (OV)* represents a segmented muon detector providing (x, y)-information. An upper and a lower layer are mounted at a relative distance of 3.9 m, allowing to reconstruct muon tracks.

The electronics and data acquisition (DAQ) system digitalizes and stores the waveforms of the ID and IV PMTs dead-time free. As both the ID and IV channels are read out upon any trigger in either of the two sub-detectors, background events entering the ID from outside can be tagged and vetoed.

The ID volumes can be accessed through a *chimney*,

located at the top of the detector in the center. Encapsulated sources of the radioactive isotopes ^{137}Cs, ^{68}Ge, ^{60}Co and ^{252}Cf can be inserted for calibration purposes.

A multi-wavelength LED system is used to regularly calibrate the readout electronics. Spallation neutrons and ^{212}Bi-^{212}Po coincidences introduced by radioimpurities are used to study the detector response and related systematic uncertainties.

As the ND was under construction in the first phase of the experiment, the current DC analysis is based on the data recorded with the FD. The parameter θ_{13} is obtained from the comparison of the measured neutrino rate and energy spectrum to a prediction calculated by a Monte Carlo (MC) simulation. Hence, the accuracy of the simulated energy scale represents an important aspect. To achieve this requirement, the calorimetric estimation of the visible energy E_{vis} is calibrated for both detector data and MC simulation, yielding a linear, time independent and spatial uniform energy response. In a *linearized PE calibration* the number of detected photoelectrons (PE) is computed from the charge contained in a PMT signal, taking into account charge and time dependence of the conversion factor. The position dependency of the PE response is removed by a 2D correction and the energy unit converted to MeV. Another calibration step reduces time variations in the response of the detector data. Non-linear discrepancies in the data and MC energy scales are accounted for by additional corrections applied to the MC simulation. A correction handling readout and charge integration related non-linearities is preformed on any event type. The remaining non-linearity is introduced by the scintillation modeling and therefore particle dependent. The corresponding correction is hence only applied to IBD positron candidates. In total a systematic energy scale uncertainty of 0.74 % is achieved, weighted over the prompt energy spectrum.

3. Neutrino Candidate Selection

The neutrino candidate sample is selected after the rejection of muons, events occurring within less than 1 ms time difference to the last preceding muon and triggers induced by sporadic light emission from the PMT bases (so-called *light noise*) [2]. The cuts were developed to remove light noise events based on the inhomogeneous charge detection and signal pulse timing in the ID PMTs. The candidate selection is based on the search for a two-fold coincidence signal with the following cuts: 1) a prompt energy of $0.5 < E_{\text{vis}} < 20\,\text{MeV}$ is required, 2) the delayed event should deposit an energy of $4 < E_{\text{vis}} < 10\,\text{MeV}$, 3) the correlation time between prompt and delayed has to satisfy $0.5 < \Delta t_{\text{corr}} < 150\,\mu\text{s}$, 4) the prompt-delayed correlation distance has to be smaller than 1 m and 5) no other trigger besides the delayed event occurs $200\,\mu\text{s}$ before and $600\,\mu\text{s}$ after the prompt event.

Owing to the extended selection windows compared to the previous DC analysis [2], the detection efficiency is increased and related data to MC discrepancies reduced. As the prompt detection occurs with a trigger efficiency of about 100 % and negligible uncertainty, the detection efficiency of the IBD signal and its uncertainty is dominated by the delayed event detection. The latter is measured with neutrons from ^{252}Cf fission and IBD reaction using new analysis techniques. The results of both independent analyses are combined and yield a detection systematic uncertainty reduced by factor 2 compared to the last publication.

Using MC simulation of IBDs the selection efficiency (without selection cut 5)) was found to have increased to 98.4 % compared to the previous analysis' efficiency of 91.2 %, while the efficiency was estimated relative to a loosened selection of $3.5 < E_{\text{delayed}} < 12\,\text{MeV}$, $0.25 < \Delta t < 1000\,\mu\text{s}$ and no constraint on the correlation distance.

Backgrounds passing the coincidence criteria of the IBD selection can be split in two classes: 1) *accidental background events*, which are false coincidences consisting of two uncorrelated events; 2) *correlated backgrounds*, which subdivide in fast neutrons, long-lived cosmogenic isotopes such as the β-n emitters ^{9}Li and ^{8}He, and stopping muons decaying in the ID.

The accidental background rate and spectral shape can be measured with high precision selecting uncorrelated delayed candidates with 1 s offset to a prompt event. In order to increase the statistics further, successive background measurement windows were added.

Most of the correlated backgrounds relevant for the DC analyses are muon-induced. Their correlation to the parent muon can therefore either be used to study rate and shape of the backgrounds or further reduce their contribution by means of newly developed vetoes (see Section 4) on the analysis level. The rate of the cosmogenic β-n emitters is studied by searching after highly energetic muons for events decaying with lifetimes of $\tau = 257\,\text{ms}$ (^{9}Li) and $\tau = 172\,\text{ms}$ (^{8}He). Reduction in the systematic uncertainty of the rate estimation was achieved by the selection of a background sample with enhanced purity. Event-by-event selection of ^{9}Li+^{8}He became possible by the application of a likelihood-based identification algorithm, which was

Background source	Rate (d^{-1})	Gd-III/Gd-II
^{9}Li+^{8}He	$0.97^{+0.41}_{-0.16}$	0.78
Fast-n, Stopping-μ	0.604 ± 0.051	0.52
Accidental	0.070 ± 0.003	0.27
^{13}C(α, n)^{16}O	< 0.1	N/A
^{12}B	< 0.03	N/A

Table 1: Background rate estimations of the current analysis (Gd-III) [1] (systematic uncertainties included) and reduction with respect to the previous publication (Gd-II) [2]. The computation of Gd-III/Gd-II takes the different selection criteria into account. The ^{13}C(α, n)^{16}O and ^{12}B backgrounds were not addressed by Gd-II.

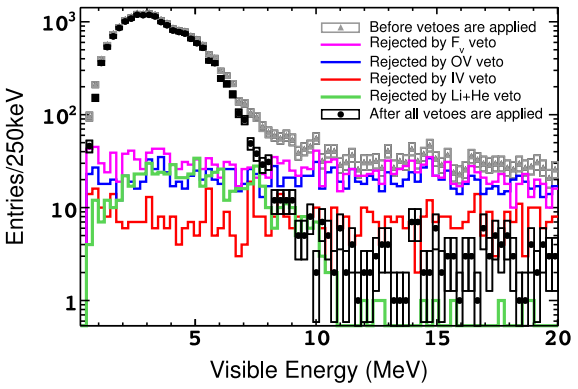

Figure 2: Prompt signal visible energy. The data points represent the measured spectra and their statistical uncertainty before (gray, triangle) and after (black, circle) the F_V, OV, IV and ^{9}Li+^{8}He likelihood veto were applied in combination. The colored lines show the candidates rejected by each individual veto: F_V veto (magenta), OV veto (blue), IV veto (red) and ^{9}Li+^{8}He likelihood veto (green).

used to extract the spectral shape from data [11].

In the case of the fast neutron and stopping muon backgrounds the parent muons either miss the active detector areas or deposit not enough energy to be identified. The muon track or the spallation and decay products however deposit often energy in the IV scintillator and can therefore be tagged. This tagging technique (the *IV veto cut*, Section 4) was used to extract the fast neutron and stopping muon energy spectrum. A flat spectrum was measured and confirmed by studies using different selection cuts and the OV information. From the coincidence signals observed in the energy region $20 < E_{\mathrm{vis}} < 30$ MeV the fast neutron and stopping muon rate was estimated.

Other backgrounds including the ^{13}C(α, n)^{16}O reaction and ^{12}B coincidences were studied and found to occur with negligible rates. A summary of the background rate estimation and reduction with respect to the previous publication [2] is given in Table 1.

4. New Background Vetoes

While accidental backgrounds are suppressed by the requirement of a prompt event to occur in coincidence with a ∼8 MeV neutron capture on Gd, new veto cuts are applied along with the standard IBD selection, reducing the rate of correlated backgrounds (Fig. 2).

If a prompt trigger coincides with an OV trigger within 224 ns, it is rejected from the IBD sample. The upper and lower OV systems were installed for 27.6 % of the data set presented in this article. For 56.7 % of the data was recorded only with the lower OV, for the remaining 15.7 % no OV was available.

The *IV veto* condition rejects IBD candidates in case the prompt event and an IV energy deposition of more than 0.2 MeV detected by at least 2 IV PMTs occur within less than 50 ns time difference. By requiring the distance between the ID and IV reconstructed vertices to be less than 3.7 m, the exclusion of accidental coincidences of IV and IBD events is reduced.

An effective way to identify stopping muons is to use the likelihood output value F_V of the vertex reconstruction as measure for the dissimilarity of the delayed event and a point-like light source. Since stopping muons mainly enter the ID through the chimney, their PMT hit patterns deviates from the one created by common physics events. A 2D cut on the delayed visible energy rejecting events with $E_{\mathrm{vis}} < 0.068 \cdot \exp(F_V/1.23)$ succeeds to reduce the stopping muon contribution. Whereas the fast neutron and stopping muon contributions were of comparable size in the last analysis, their combined rate is after the F_V *veto* cut mainly represented by fast neutron events.

The decays of cosmogenic isotopes are vetoed by means of a *^{9}Li+^{8}He likelihood*, removing about 55 % of this correlated background type. It is based on information of the lateral distance to the parent muon as well as the number of neutrons created along with the ^{9}Li+^{8}He candidates.

A showering muon veto applied in the last analysis extended the veto time after a high energy muon to 0.5 s. As a consequence the dead time increased from 4.5 % to 9.2 %. Due to the improvements achieved in the background rejection, this showering muon cut could be abandoned in the analyses presented here.

For energies larger than 12 MeV no neutrino signal is expected. In this background dominated region the combination of the OV, IV and F_V vetoes reject about 90 % of the IBD candidates selected without any veto applied.

	Uncert. (%)	Gd-III/Gd-II
Reactor flux	1.7	1
Detection Efficiency	0.6	0.6
^{9}Li+^{8}He BG	+1.1 / −0.4	0.5
Fast-n, Stopped-μ BG	0.1	0.2
Statistics	0.8	0.7
Total	+2.3 / −2.0	0.8

Table 2: Signal and background normalization uncertainties relative to the signal prediction [2, 1]. The last column represents the relative reduction Gd-III/Gd-II with respect to the previous analysis.

5. Oscillation Analysis Results

In 460.67 live days of the reactor on phase 17351 IBD candidates were selected, while 18290 were expected. This deficit in measured IBD reactions compared to the prediction is interpreted as consequence of neutrino flavor oscillations induced by a non-zero value of the mixing angle θ_{13}.

Owing to the experimental configuration featuring only two reactor cores, the DC experiment experiences the unique opportunity to take data while both reactors are turned off. This special condition allows for a background measurement in the absence of a neutrino signal. In total 7.24 days of reactor-off data was collected in 2011 and 2012 [13]. The predicted number of IBD candidates including residual $\bar{\nu}_e$ events is $12.9^{+3.1}_{-1.4}$, while 7 were observed. Both numbers are compatible at 9.0 % (1.7 σ).

The *Rate+shape (R+S) analysis* exploits the energy dependence of the neutrino oscillation deficit by extraction of θ_{13} from the comparison of the measured rate and spectral shape to a MC prediction (Fig. 3). The prompt selection window was extended to energy regions which are background dominated, constraining the backgrounds in the θ_{13} fit further. Compared to the previous publications, a measured ^{238}U spectrum was included in the current reactor prediction [12]. While in past analyses the reactor-off data had been used to crosscheck the background estimates, the amount of collected data had increased and was included in the oscillation analysis. In Table 2 the normalization uncertainties of signal and background relative to the signal prediction are summarized.

The prompt spectrum is separated in energy bins of variable sizes, background rates and spectral shapes are retrieved from the background studies described in Section 3. Statistical and systematic uncertainties are propagated in the fit using covariance matrices, taking bin-to-bin correlations into account. Additional

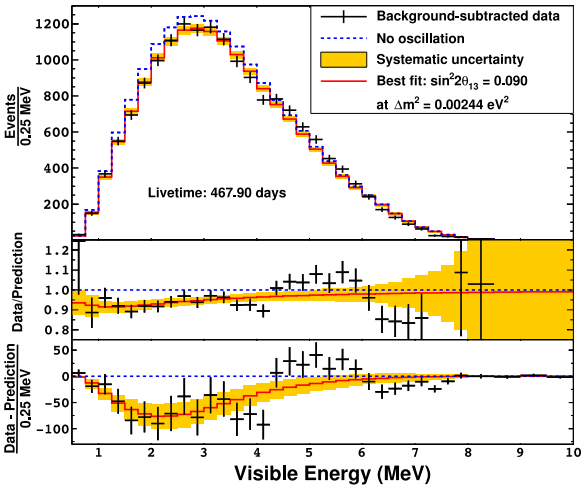

Figure 3: Observed IBD candidate spectrum (black points), while the backgrounds were subtracted using the R+S fit outputs for normalization. The no-oscillation prediction (blue dashed line) and the predicted oscillated spectrum (red line) at the R+S best fit value of θ_{13} are superimposed. Bottom panels: differences between the data and the no-oscillation prediction (data points), and differences between the best-fit prediction and the no-oscillation prediction (red curve). The orange band corresponds to the systematic uncertainties on the best-fit prediction.

parameters related to the energy scale, correlated background rates and the value of Δm^2_{31} were allowed to vary in the fit, correcting the neutrino prediction for possible systematic effects. A χ^2 statistics is scanned in $\sin^2 2\theta_{13}$ minimizing over the correction parameters, while constraints on these parameters were given by their uncertainties. The best fit value is found at $\sin^2 2\theta_{13} = 0.090^{+0.032}_{-0.029}$ (stat + syst) with $\chi^2_{\rm min}/{\rm NDF} = 52.2/40$. The fit output value of the background rate amounts to (1.38 ± 0.14) events per day, in agreement with the estimations of Table 1. The background rate uncertainty reduces due to additional information obtained from the energy spectral shape.

Another fit framework takes advantage of the variations that the DC experiment observes in thermal power. In the *Reactor Rate Modulation (RRM) analysis* [10] the data is separated in seven data points according to the reactor power conditions: three data points correspond to both reactors turned on, another set of three data points is related to intermediate power (one reactor is off) and a last data point represents the background-only measurement (both reactors off). Once the daily rate of observed candidates is plotted as a function of the expected daily neutrino rate (Fig. 4), the mixing angle θ_{13} can be extracted from the slope of a straight line

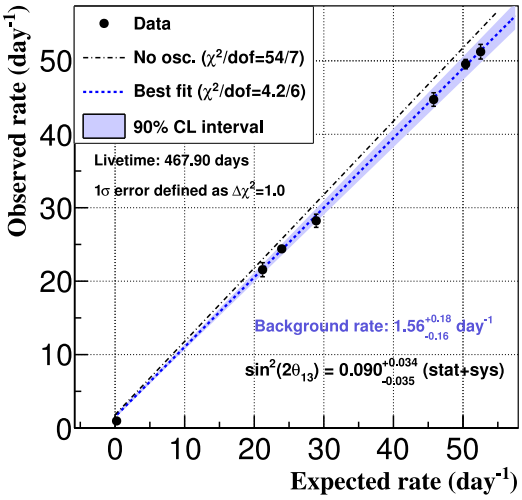

Figure 4: Correlation of the measured daily candidate rate and the expected daily neutrino rate. The blue line corresponds to the best RRM fit. In this analysis the reactor-off point (first data point) and the background estimates were included.

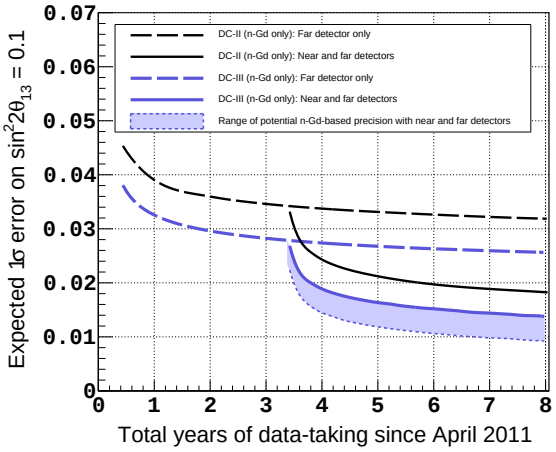

Figure 5: The projected sensitivity of Double Chooz for an analysis using the neutron detection channel on Gd.

fit to the data. At the same time, the daily background rate B is represented by the intercept of the fitted line. Furthermore a background-model-independent measurement of θ_{13} is possible, depending on the constraints added to the RRM analysis.

With an additional constraint on the background rate of $B^{\rm exp} = 1.64^{+0.41}_{-0.17}\,{\rm d}^{-1}$ obtained from background measurements, the RRM analysis yields $\sin^2 2\theta_{13} = 0.090^{+0.034}_{-0.035}$, which is in excellent agreement with the R+S result. After the fit the background rate amounts to $B = 1.56^{+0.18}_{-0.16}\,{\rm d}^{-1}$, consistent with the background estimation.

In the case of a background unconstraint fit, the results are given by $\sin^2 2\theta_{13} = 0.060 \pm 0.039$ and $B = 0.93^{+0.43}_{-0.36}\,{\rm d}^{-1}$. The impact of the reactor-off measurement on the θ_{13} precision is studied by removing both the background constraint and the reactor-off term, then $\sin^2 2\theta_{13} = 0.089 \pm 0.052$ and $B = (1.56 \pm 0.86)\,{\rm d}^{-1}$ are obtained.

As the current DC analyses were based on a single detector measurement, the precision of the θ_{13} result is limited by the uncertainty on the reactor flux. In the near future the ND+FD phase will lead to a cancellation of the correlated uncertainties between the two detectors and an immediate improvement in the experiment's sensitivity. In Fig. 5 the projected sensitivity of a Gd-based analysis with either one detector or both the FD and ND is shown. The sensitivity curves are given with respect to the previous Gd-II (black) [2] and the current Gd-III (blue) [1] analysis, depicting the progress made by the Gd-III analysis. For the ND+FD analysis a 0.1 % uncertainty on the reactor flux, 0.2 % uncertainty on the detection efficiency and background uncertainties scaled from FD to ND are assumed. Along with further improvements on the analysis techniques and systematics a sensitivity in the shaded area could be reached, while the lower edge corresponds to the case in which the reactor flux would represent the only contribution to the systematic uncertainty.

6. Spectrum Distortion

The energy dependence of the neutrino oscillation is illustrated in Fig. 3 in the lower panels. There, the ratio of the background subtracted data to the unoscillated prediction is shown as a function of the prompt visible energy. The deficit below 4 MeV is interpreted as observation of electron antineutrino disappearance. A spectrum distortion is found above 4 MeV, characterized by an excess for energies up to 6 MeV and a deficit around 7 MeV. This spectral distortion does not affect the θ_{13} measurement and crosschecks have shown that the excess at 4.25 – 6 MeV is correlated to the reactor power, disfavoring backgrounds as possible origin.

A distortion of the antineutrino spectrum was first reported by the DC experiment and confirmed by the reactor neutrino experiments Daya Bay and RENO.

7. Conclusion

The DC experiment measured an energy dependent deficit in the flux of reactor antineutrinos. This information is used to extract the mixing angle θ_{13}.

Improvements in the signal selection, calibration techniques and the increase of accumulated statistics reduced the uncertainties on energy response, background rates and detection efficiency. The current best result of the DC experiment is given by the R+S fit of the Gd-channel analysis with $\sin^2 2\theta_{13} = 0.090^{+0.032}_{-0.029}$ (stat + syst). Analyses of a second fit framework evaluating the same data set with a different approach to extract θ_{13}, yields consistent results. A spectral distortion was observed in the prompt energy spectrum at hight energies not affecting the θ_{13} result. After three years of running with two detectors, $\sigma(\sin^2 2\theta_{13}) = 0.015$ should be reached. The sensitivity could be further improved to 0.010, depending on the improvements made on the analysis.

References

[1] Y. Abe *et al.*, arXiv:1406.7763v2 [hep-ex] (2014).
[2] Y. Abe *et al.*, Phys. Rev. D86, 052008 (2012).
[3] Y. Abe *et al.*, Phys. Lett. B723, 66 (2013).
[4] J. Beringer *et al.*, Phys. Rev. D86, 010001 (2012) and 2013 partial update for the 2014 edition.
[5] E. P. An *et al.*, Phys. Rev. Lett. 112, 061801 (2014).
[6] J. K. Ahn *et al.*, Phys. Rev. Lett. 108, 191802 (2012).
[7] P. Adamson *et al.*, Phys. Rev. Lett. 110, 171801 (2013).
[8] J. K. Ahn *et al.*, Phys. Rev. Lett. 112, 061802 (2014).
[9] P. Adamson *et al.*, Phys. Rev. Lett. 112, 191801 (2014).
[10] Y. Abe *et al.*, Phys.Lett. B735, 51 (2014).
[11] Y. Abe *et al.*, Nucl. Instr. Meth. A. 764, 330 (2014).
[12] N. Haag *et al.*, Phys. Rev. Lett. 112, 122501 (2014).
[13] Y. Abe *et al.*, Phys. Rev. D87, 011102 (2013).